

Error analysis of first time to a threshold value for partial differential equations

Jehanzeb H. Chaudhry Don Estep Trevor Giannini Zachary Stevens
Simon Tavenier

November 19, 2021

Abstract

We develop an *a posteriori* error analysis for a novel quantity of interest (QoI) evolutionary partial differential equations (PDEs). Specifically, the QoI is the first time at which a functional of the solution to the PDE achieves a threshold value signifying a particular event, and differs from classical QoIs which are modeled as bounded linear functionals. We use Taylor’s theorem and adjoint based analysis to derive computable and accurate error estimates for linear parabolic and hyperbolic PDEs. Specifically, the heat equation and linearized shallow water equations (SWE) are used for the parabolic and hyperbolic cases, respectively. Numerical examples illustrate the accuracy of the error estimates.

1 Introduction

The first time a certain quantity in a physical system reaches a threshold value is often of interest. Such physical systems are often modeled by differential equations. Important examples of this quantity of interest (QoI) in a partial differential equation (PDE) framework include the first time at which the temperature in a specified domain reaches a threshold, the momentum of the ocean in a particular area indicates a possible tsunami, the concentration of a chemical leaching into groundwater becomes toxic, etc. In this article, we consider linear evolutionary PDEs of the form

$$u_t(x, t) + Lu(x, t) = f(x, t), \quad x \in \Omega, \quad t \in (t_0, T] \quad (1)$$

where $u_t = \frac{\partial u}{\partial t}$, L is a linear differential operator in x , and $f(x, t)$ is a continuous function. The functions u and f can be scalar or vector valued. The assumption of linearity is chosen to avoid issues of well-posedness of the solution to (1), however, the analysis we develop is easily extendable to nonlinear PDEs as demonstrated in Appendix A. Let $S[u](t)$ be a time-dependent linear functional of $u(x, t)$ and let R be a threshold value. With the functional and threshold value let $Q(u)$ be the aforementioned QoI. That is, $Q(u)$ is the first time at which the relation $S[u](t) = R$ is satisfied. Assuming that such a $t < T$ exists, $Q(u)$ has the form

$$Q(u) = \min\{t \in (t_0, T] | S[u](t) = R\}. \quad (2)$$

Classical *a posteriori* error analysis deals with QoIs that can be expressed as bounded functionals of the solution and has been widely explored [1–4, 6–13, 15, 16, 19–21, 24, 26, 28, 30, 31, 35]. The error estimation utilizes generalized Green’s functions solving an adjoint problem, computable residuals of the numerical solution, and variational analysis [1, 4, 21, 27, 30, 31]. The error estimation method is usually used in conjunction with a finite element or variational method, however numerous finite difference/volume methods are applicable provided they be recast as an equivalent finite element method [8, 12, 19, 20, 22, 23, 25, 29, 36]. Nonlinear QoIs are typically handled by linearization around a computed solution [4, 7, 18]. We refer to the QoI covered by the classical analysis as ‘standard’. A quantity of the form (2) cannot be expressed as a bounded linear functional of u , nor can it be trivially linearized, and hence we refer to this $Q(u)$ as a ‘non-standard QoI’.

Recent work in [17] applied *a posteriori* error analysis for such a QoI under the framework of ordinary differential equations (ODEs). In this work, we extend that analysis to evolutionary PDEs. The error estimate is derived using Taylor series, linearizing around a computed QoI. It is then made computable

through the use of solutions to certain adjoint problems. When expanding from linear ODEs to linear PDEs, the error estimate requires one additional adjoint problem.

The evolutionary PDEs examined are the heat equation and the linearized shallow water equations (SWE). The heat equation models the diffusion of heat or concentration of some chemical throughout a domain. The linearized SWE model wave and flow propagation in a fluid in a domain where the horizontal scale is much larger than the vertical scale. In principle, any fluid in a domain where this difference in scale is respected can be modeled by the linearized SWE. Commonly, these equations are applied to dams, oceans, the atmosphere, etc. In these cases, the linearized SWE can be used to model tsunami wave propagation, inundation in coastal areas due to a tsunami, flooding from a dam break, and atmospheric waves and flows [5, 33]. Standard QoIs for the linearized SWE have been studied previously in [21] and this work is extended in this paper to non-standard QoIs for the linearized SWE.

In §2, we lay out the weak-form of (1) and discuss a class of numerical schemes used to solve variational problems. The error analysis for the non-standard QoI is detailed in §3. We start by presenting a classical result in §3.3. The main theorem of the article is presented in §3.1, where we derive a representation of the error in the QoI (2), the proof of which takes advantage of Taylor's theorem and the variational form of the PDE. The non-computable terms in our representation are then approximated to get a computable error estimate in §3.2. The computable estimates are applied to examples of parabolic and hyperbolic PDEs in §4.1 and §4.2, respectively. Finally, numerical results are presented in §5.

2 Variational Formulations and Numerical schemes

Adjoint-based, *a posteriori* error estimates utilize the variational (or weak) form of PDEs. This section details the general weak form of (1) and the specific weak forms of certain example PDEs. Variational space-time Galerkin finite element methods, used for the numerical solution of PDEs, are also presented.

2.1 Variational Formulations

Let W be a generic Hilbert space over the domain Ω with inner product $\|\cdot\|_W$, and let $L^2(t_0, T; W)$ denotes the space of functions w whose W -norm is square integrable over the time interval $[t_0, T]$, that is, $\int_0^T \|w(\cdot, t)\|_W^2 dt < \infty$. The variational form of (1) is: find $u \in L^2(t_0, T; W)$ such that

$$\langle u_t(\cdot, t), v(\cdot, t) \rangle + (L_1 u(\cdot, t), L_2 v(\cdot, t)) = (f(\cdot, t), v(\cdot, t)), \quad \forall v \in W, \quad \forall t \in (t_0, T] \quad (3)$$

where $\langle \cdot, \cdot \rangle$ denotes the duality pairing of W and its dual space W^* , $(a, b) = \int_\Omega a \cdot b \, d\Omega$ is the spatial L^2 inner product over Ω . The two operators L_1, L_2 are linear differential operators such that $L_2^* L_1 u = Lu$. The operator L_2^* is the formal adjoint of L_2 which satisfies the property that

$$(u, L_2 v) = (L_2^* u, v), \quad \text{for all } u \in W, v \in W. \quad (4)$$

Under suitable conditions on the operators L_1 and L_2 (and hence L), (3) is well-posed; we refer the reader to [32] for more details. The differential operator L_1 may be of lower order than L . Although, if a solution u to (3) is sufficiently differentiable, it will also satisfy (1).

As specific examples of PDEs of the form (1), we focus on the heat equation and a linearized version of the shallow water equations, representing examples of parabolic and hyperbolic PDEs respectively. The following sections present the weak forms of these PDEs. In particular, describing the operators L, L_1 , and L_2 , the solution space W , and the dual space W^* .

2.1.1 Heat Equation

Consider the inhomogeneous heat equation over a domain $\Omega \subset \mathbb{R}^n$

$$u_t(x, t) - \nabla^2 u(x, t) = f(x, t), \quad x \in \Omega, \quad t \in [t_0, T], \quad (5)$$

where $u(x, t)$ is the temperature of the medium. In the notation of (1), the heat equation has the operator $L = -\nabla^2$. For any function $v \in H_0^1(\Omega) \cap H^2(\Omega)$,

$$(Lu, v) = (-\nabla^2 u, v) = (\nabla u, \nabla v) \quad (6)$$

implying $L_1 = \nabla = L_2$. The weak form is: Find $u \in L^2(t_0, T; H^1(\Omega))$

$$\langle u_t, v \rangle + (\nabla u, \nabla v) = (f, v) \quad \forall v \in H_0^1(\Omega), \quad t \in (t_0, T). \quad (7)$$

2.1.2 Linearized Shallow Water Equations

The other problem under consideration is the linearized shallow water equations with perfectly reflective boundaries. Start with the nonlinear shallow water equations in 1D:

$$\begin{aligned} \eta_t(x, t) + \mu_x(x, t) &= f_1(x, t), \\ \mu_t(x, t) + \left(\frac{\mu(x, t)^2}{\eta(x, t)} + \frac{1}{2} g \eta(x, t)^2 \right)_x + g \eta B_x(x) &= f_2(x, t). \end{aligned} \quad (8)$$

The solution is $\vec{u}(x, t) = (\eta(x, t), \mu(x, t))^\top$, where $\eta(x, t)$ corresponds to the water surface elevation, $\mu(x, t)$ corresponds to the momentum of the fluid. The constant g is the gravitational acceleration constant. In most physical situations the right hand side $\vec{f}(x, t) = (f_1(x, t), f_2(x, t)) = \vec{0}$. This corresponds to cases where the situation of interest is how an initial state, such as a dam break, initial tsunami wave, etc. propagates. However, for the manufactured solutions method used for verification, it will not be zero in general. In that case, the right hand side will be the true solution chosen and plugged into the PDE.

Linearizing (8) around a flat surface, a fluid with no deviations in the height of the surface such as preexisting waves, with elevation $\bar{\eta}$ and momentum $\bar{\mu} = 0$, the fluid is at rest with regards to movement of the fluid, (see [21]) yields

$$\begin{aligned} \eta_t(x, t) + \mu_x(x, t) &= f_1(x, t), \\ \mu_t(x, t) + g \bar{h}(x) \eta_x(x, t) &= f_2(x, t), \end{aligned} \quad (9)$$

where $\bar{h}(x) = \bar{\eta} - B(x)$. Here, the operator L is

$$L = \begin{pmatrix} 0 & \frac{\partial}{\partial x} \\ g \bar{h}(x) \frac{\partial}{\partial x} & 0 \end{pmatrix} \quad (10)$$

Since L contains only first order derivatives, the operators L_1 and L_2 are

$$L_1 = L = \begin{pmatrix} 0 & \frac{\partial}{\partial x} \\ g \bar{h}(x) \frac{\partial}{\partial x} & 0 \end{pmatrix}, \quad L_2 = \begin{pmatrix} 1 & 0 \\ 0 & 1 \end{pmatrix}. \quad (11)$$

The weak form of (9) is: find $u \in L^2(t_0, T; H^1(\Omega))$

$$\begin{aligned} \langle \eta_t, v_1 \rangle + \langle \mu_x, v_1 \rangle + \langle \mu_t, v_2 \rangle + g \langle \bar{h} \eta_x, v_2 \rangle &= (f_1, v_1) + (f_2, v_2), \\ \forall \vec{v} = (v_1, v_2) \in H_0^1(\Omega), \quad t \in (t_0, T). \end{aligned} \quad (12)$$

2.2 Numerical Scheme: Space-Time Galerkin Finite Element Method

Let \mathcal{T}_h be a shape-regular triangulation of the spatial domain Ω where h denotes the diameter of the largest element. In one spatial dimension, \mathcal{T}_h is a uniform set of N_x subintervals of the domain where h denotes the width of the subintervals. Let $V_1^{q_s}$ be the standard space of continuous piecewise polynomials of degree q_s on \mathcal{T}_h such that if $U \in V_1^{q_s}$ then $U = 0$ on $\partial\Omega$. Let $V_2^{q_s}$ be the standard space of continuous piecewise polynomials of degree q_s on \mathcal{T}_h such that if $U \in V_2^{q_s}$ then $U_2 = 0$ on $\partial\Omega$ where U_2 is the second component of $U = (U_1, U_2)$.

The time domain $[t_0, T]$ is discretized into N_t uniform subintervals of width p denoted \mathcal{T}_p . $\mathcal{T}_p = \{I_1, \dots, I_n, \dots, I_{N_t}\}$ where $I_n = [t_n, t_{n+1}]$. Let $l_j(t)$ be the j th degree Lagrange polynomial in time on the interval I_n . For the space-time slab $S_n = \Omega \times I_n$ the solution space is defined as (see [27])

$$W_{n,i}^{q_t, q_s} = \{w(x, t) | w(x, t) = \sum_{j=0}^{q_t} l_j(t) v_j(x), v_n \in V_i^{q_s}, (x, t) \in S_n, \} \quad i \in \{1, 2\}. \quad (13)$$

The variational method used in the article is the continuous Galerkin method in space-time. The continuous Galerkin method, cG(q_t, q_s) is: find U such that it is continuous on $\Omega \times [t_0, T]$, its restriction to S_n belongs to $W_{n,i}^{q_t, q_s}$, and the restriction satisfies

$$\int_{t_n}^{t_{n+1}} \left[\left(U_t(\cdot, t), v(\cdot, t) \right) + \left(L_1 U(\cdot, t), L_2 v(\cdot, t) \right) \right] dt = \int_{t_n}^{t_{n+1}} \left(f(\cdot, t), v(\cdot, t) \right) dt, \quad \forall v \in W_{n,i}^{q_t-1, q_s}. \quad (14)$$

In addition to variational methods, many commonly used finite difference schemes, such as IMEX methods, Lax-Wendroff, Crank-Nicolson, etc. are also acceptable as they can be cast to nodally equivalent variational methods (see [9, 17, 20]).

2.3 Quantity of Interest: Time to a Threshold

The non-standard QoI is the first time at which a specified event occurs. The occurrence of the event is represented as a linear functional of the solution of (1) achieving a threshold value R , for the very first time. To formalize this, let $S[u](t)$ be a time-dependent linear functional of $u(x, t)$

$$S[u](t) = \int_{\Omega} w(x) \cdot u(x, t) d\vec{x} = (w(\cdot), u(\cdot, t)), \quad (15)$$

where $w(x)$ is some differentiable weight function. Assume that $w(x)|_{\partial\Omega} = 0$. Recall that this QoI can be written as (2).

3 A Posteriori Error Analysis

Let $u(x, t)$ be the true solution of (1) and denote the true value of the QoI $t_t := Q(u)$. Note that, in (5), u and f are scalar valued, while in (9), $u = (\eta, \mu)^\top$ and $f = (f_1, f_2)^\top$. Let $U(x, t)$ be an approximation of the solution given by the solution found in (14) and $t_c := Q(U)$ the corresponding computed QoI. See Figure 1 for an illustration of this set up. Denote the error in the approximate solution as $e(x, t) = u(x, t) - U(x, t)$. The analysis of accurately estimating the error linear functionals applied to $e(x, t)$ is well known (see [1, 2, 4, 12, 14, 18–21, 24, 28, 34]), however the subject of this article is estimating the error

$$e_Q = t_t - t_c. \quad (16)$$

This section is dedicated to deriving an accurate *a posteriori* error estimate $\nu \approx e_Q$. The accuracy of the error estimate is quantified by the effectivity ratio

$$\rho_{eff} = \frac{\nu}{e_Q}, \quad (17)$$

where $\rho_{eff} \approx 1$ indicates an accurate estimate.

An error representation is derived using multiple applications of Taylor's Theorem. The error representation is then estimated using computable residuals and solutions to certain adjoint problems as detailed in the following sections.

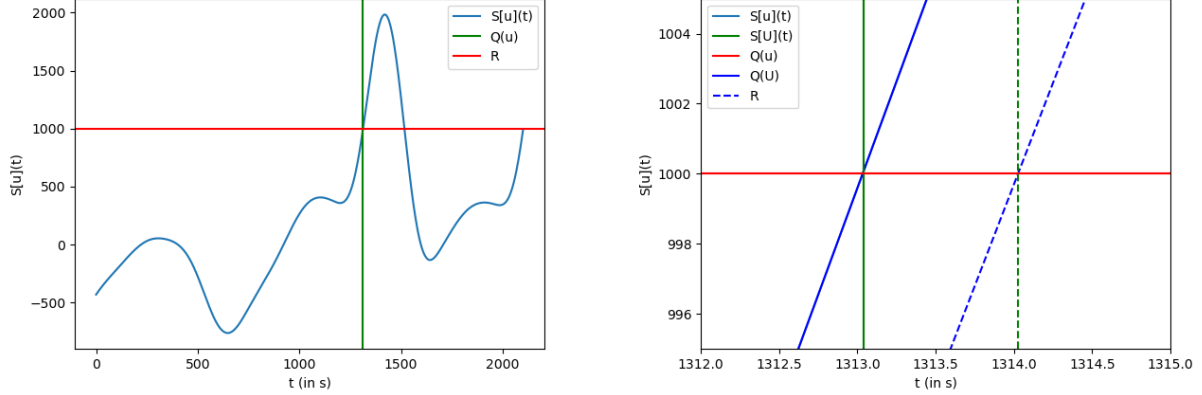
3.1 Error Formulation for PDEs

Theorem 1 provides a representation of the error (16)

Theorem 1. *For a PDE of the form (1) with weak form (3), if the function $f(x, t)$ is continuous, the error in the computed QoI (2) is*

$$e_Q = t_t - t_c = \frac{(w(\cdot), e(\cdot, t_c)) + (w(\cdot), \mathcal{R}(\cdot, t_c, t_t))}{(L_2 w(\cdot), L_1 U(\cdot, t_c)) - (w(\cdot), f(\cdot, t_c)) + (L_2 w(\cdot), L_1 e(\cdot, t_c))}. \quad (18)$$

Where $e(x, t) = u(x, t) - U(x, t)$, and the remainder is $\mathcal{R}(x, t_c, t_t) = \mathcal{O}((t_t - t_c)^2)$.



(a) Graph showing threshold value R , True functional S , and (b) Close up of true QoI and numerical QoI for example in Section 5.5

Figure 1

Proof. From the definition of the QoI (2), it follows that

$$S[u](t_t) - S[U](t_c) = R - R = 0. \quad (19)$$

Writing S as the inner-product shows that

$$(w(\cdot), u(\cdot, t_t) - U(\cdot, t_c)) = 0. \quad (20)$$

Expand $u(x, t_t)$ around t_c using Taylor Series and define $e(x, t) = u(x, t) - U(x, t)$ to obtain

$$0 = (w(\cdot), u(\cdot, t_c) + (t_t - t_c)u_t(\cdot, t_c) + \mathcal{R}(\cdot, t_c, t_t) - U(\cdot, t_c)) \quad (21)$$

$$= (w(\cdot), e(\cdot, t_c)) + (t_t - t_c)(w(\cdot), u_t(\cdot, t_c)) + (w(\cdot), \mathcal{R}(\cdot, t_c, t_t)) \quad (22)$$

where the remainder $\mathcal{R}(x, t_c, t_t)$ is of order $\mathcal{O}((t_t - t_c)^2)$. Rearrange (22) to isolate the error of interest:

$$t_t - t_c = -\frac{(w(\cdot), e(\cdot, t_c)) + (w(\cdot), \mathcal{R}(\cdot, t_c, t_t))}{(w(\cdot), u_t(\cdot, t_c))}. \quad (23)$$

Focusing on the denominator of (23), use (3) to replace the u_t . Note that, due to linearity, $L_1 u(x, t) = L_1 U(x, t) + L_1 e(x, t)$, which gives

$$(w(\cdot), u_t(\cdot, t_c)) = -(L_2 w(\cdot), L_1 u(\cdot, t_c)) + (w(\cdot), f(\cdot, t_c)) \quad (24)$$

$$= -(L_2 w(\cdot), L_1 U(\cdot, t_c)) - (L_2 w(\cdot), L_1 e(\cdot, t_c)) + (w(\cdot), f(\cdot, t_c)) \quad (25)$$

Plugging (25) into (23) yields the final result

$$t_t - t_c = \frac{(w(\cdot), e(\cdot, t_c)) + (w(\cdot), \mathcal{R}_1(\cdot, t_c, t_t))}{(L_2 w(\cdot), L_1 U(\cdot, t_c)) - (w(\cdot), f(\cdot, t_c)) + (L_2 w(\cdot), L_1 e(\cdot, t_c))}. \quad (26)$$

□

See 3 in Appendix A for error representation in the case when f may also depend on the solution u , possibly in a nonlinear manner.

3.2 Error Estimate

In the error representation (18), the magnitude of the remainder \mathcal{R}_1 decreases faster than other terms as the numerical solution becomes more accurate. Setting $(w(\cdot), \mathcal{R}_1(\cdot, t_c, t_t)) \approx 0$ gives the first approximation

$$t_t - t_c \approx \frac{(w(\cdot), e(\cdot, t_c))}{(L_2 w(\cdot), L_1 U(\cdot, t_c)) - (w(\cdot), f(\cdot, t_c)) + (L_2 w(\cdot), L_1 e(\cdot, t_c))}. \quad (27)$$

The approximation (27) contains the error $e(x, t) = u(x, t) - U(x, t)$ which is not directly computable. One way to deal with the terms containing $e(x, t)$ is by using classical adjoint-based error analysis as detailed in Theorem 2.

3.3 A classical *a posteriori* error representation

Theorem 2. *Given a numerical solution $U(x, t)$ to (3) and data $\psi(x)$, the error $(\psi(\cdot), e(\cdot, \hat{t}))$ for $\hat{t} \in (t_0, T]$ is given by*

$$(\psi(\cdot), e(\cdot, \hat{t})) = (\phi(\cdot, t_0), e(\cdot, t_0)) + \int_{t_0}^{\hat{t}} (\phi(\cdot, \hat{t}), f(\cdot, \hat{t}) - U_t(\cdot, \hat{t})) dt - \int_{t_0}^{\hat{t}} (L_2 \phi(\cdot, \hat{t}), L_1 U(\cdot, \hat{t})) dt \quad (28)$$

where $\phi(x, t)$ is the solution of the adjoint problem

$$\begin{aligned} -\phi_t(x, t) &= L^* \phi(x, t), \quad x \in \Omega, \quad t \in [t_0, \hat{t}) \\ \phi(x, t)|_{\partial\Omega} &= 0, \quad t \in [t_0, \hat{t}), \\ \phi(x, \hat{t}) &= \psi(x), \quad x \in \Omega. \end{aligned} \quad (29)$$

The linear differential operator L^* is the adjoint operator of L in (1) with property (4). Note that the adjoint problem is solved backwards in time with the initial condition given at $t = \hat{t}$. The proof is standard, however we include it for completeness.

Proof. Start with the equation

$$-\phi_t(x, t) - L^* \phi(x, t) = 0. \quad (30)$$

Multiply by the function $e(x, t) = u(x, t) - U(x, t)$, and integrate over the spatial domain Ω and the time interval (t_0, \hat{t}) :

$$-\int_{t_0}^{\hat{t}} (\phi_t(\cdot, t), e(\cdot, t)) dt - \int_{t_0}^{\hat{t}} (L^* \phi(\cdot, t), e(\cdot, t)) dt = 0. \quad (31)$$

From our decomposition of $L = L_2^* L_1$, write $L^* = L_1^* L_2$ and use the property of the adjoint L_1^* to get

$$(L^* \phi(\cdot, t), e(\cdot, t)) = (L_2 \phi(\cdot, t), L_1 e(\cdot, t)). \quad (32)$$

Enforcing zero boundary conditions on ϕ , $\phi(x)|_{\partial\Omega} = 0$, ensures that (32) does not contain boundary terms. Now, integrate the first term of (31) by parts in time and enforce the initial condition $\phi(x, \hat{t}) = \psi(x)$:

$$0 = \int_{t_0}^{\hat{t}} (\phi(\cdot, t), e_t(\cdot, t)) dt - (\phi(\cdot, \hat{t}), e(\cdot, \hat{t})) + (\phi(\cdot, t_0), e(\cdot, t_0)) - \int_{t_0}^{\hat{t}} (L_2 \phi(\cdot, t), L_1 e(\cdot, t)) dt, \quad (33)$$

$$= \int_{t_0}^{\hat{t}} (\phi(\cdot, t), e_t(\cdot, t)) dt - (\psi(\cdot), e(\cdot, \hat{t})) + (\phi(\cdot, t_0), e(\cdot, t_0)) - \int_{t_0}^{\hat{t}} (L_2 \phi(\cdot, t), L_1 e(\cdot, t)) dt. \quad (34)$$

Isolating the term of interest and expanding $e(x, t) = u(x, t) - U(x, t)$ inside the time integrals gives

$$(\psi(\cdot), e(\cdot, \hat{t})) = (\phi(\cdot, t_0), e(\cdot, t_0)) + \int_{t_0}^{\hat{t}} (\phi(\cdot, t), e_t(\cdot, t)) dt - \int_{t_0}^{\hat{t}} (L_2 \phi(\cdot, t), L_1 e(\cdot, t)) dt, \quad (35)$$

$$= (\phi(\cdot, t_0), e(\cdot, t_0)) + \int_{t_0}^{\hat{t}} (\phi(\cdot, t), u_t(\cdot, t) - U_t(\cdot, t)) dt - \int_{t_0}^{\hat{t}} (L_2 \phi(\cdot, t), L_1 u(\cdot, t) - L_1 U(\cdot, t)) dt. \quad (36)$$

Using the weak form (3) to replace the true solution u gives the desired result. \square

See Theorem 4 in Appendix A for the case when f may depend on the solution u , possibly in a nonlinear manner.

This theorem formulates the strong form of the adjoint problem (29), but ϕ only needs to satisfy the weak form of the problem

$$-(\phi(\cdot, t), v(\cdot, t)) - (L_2 \phi(\cdot, t), L_1 v(\cdot, t)) = 0 \quad \forall t \in [t_0, \hat{t}], \quad (37)$$

in order to be able to compute (28).

In practice, (28) cannot be obtained exactly because the solution ϕ will be a numerically computed solution. To account for this, the adjoint problem (37) is solved using a more accurate method than the forward problem (3).

Theorem 2 gives a way to compute the terms of (27) that contain $e(x, t)$. For each term, a problem of the form (29) must be solved using $\hat{t} = t_c$ and the appropriate initial condition $\psi(x)$.

First adjoint problem To estimate $(w(\cdot), e(\cdot, t_c))$ solve (29) with initial condition $\psi(x) = \psi^{(1)}(x) = w(x)$. Using the solution $\phi^{(1)}$ in (28) yields

$$\mathcal{E}_1 \approx (\psi^{(1)}(\cdot), e(\cdot, t_c)) = (w(\cdot), e(\cdot, t_c)). \quad (38)$$

Second adjoint problem To estimate $(L_2 w(\cdot), L_1 e(\cdot, t_c))$, assume that $w(x)$ is smooth enough for $L^* w$ to be well-defined and solve (29) with initial condition $\psi(x) = \psi^{(2)}(x) = L^* w(x)$. Using the solution $\phi^{(2)}$ in (28) yields

$$\mathcal{E}_2 \approx (\psi^{(2)}(\cdot), e(\cdot, t_c)) = (L^* w(\cdot), e(\cdot, t_c)) = (L_2 w(\cdot), L_1 e(\cdot, t)). \quad (39)$$

In the case when f may also depend on the solution u , a third adjoint is required, see (70) in Appendix A.

4 Error Estimates for Heat and Shallow Water Equations

In this section, we apply the abstract theory developed in Section 3 to the heat equation and shallow water equations.

4.1 Heat Equation

The error estimate (27) applied to the heat equation (5) becomes

$$t_t - t_c \approx \frac{(w(\cdot), e(\cdot, t_c))}{(\nabla w(\cdot), \nabla U(\cdot, t_c)) - (w(\cdot), f(U, \cdot, t_c)) + (\nabla w(\cdot), \nabla e(\cdot, t_c))}. \quad (40)$$

The two adjoint problems laid out in Section 3.3 take the form

$$\begin{aligned} \phi_t^{(i)}(x, t) - \nabla^2 \phi^{(i)}(x, t) &= 0, \\ \phi^{(i)}(x_0, t) &= \phi^{(i)}(X, t) = 0, \\ \phi^{(i)}(x, t_c) &= \psi^{(i)}(x), \end{aligned} \quad (41)$$

with the initial conditions

$$\psi^{(1)}(x) = w(x), \quad \psi^{(2)}(x) = \nabla^2 w(x). \quad (42)$$

4.2 Linearized Shallow Water Equation

For the linearized shallow water equations (9), the estimate (27) becomes

$$t_t - t_c \approx \frac{(\vec{w}(\cdot), \vec{e}(\cdot, t_c))}{\left(\vec{w}(\cdot), A(x)\vec{U}_x(\cdot, t_c)\right) - \left(\vec{w}(\cdot), \vec{f}(\cdot, t_c)\right) + (\vec{w}(\cdot), A(x)\vec{e}_x(\cdot, t_c))}, \quad (43)$$

where $\vec{f} = (f_1, f_2)^\top$, $A(x) = \begin{pmatrix} 0 & 1 \\ gh(x) & 0 \end{pmatrix}$, and $\vec{u} = (\eta, \mu)^\top$.

The adjoint problems take the form

$$\begin{aligned} \vec{\phi}_t^{(i)}(x, t) + A^\top(x)\vec{\phi}_x^{(i)}(x, t) &= 0, \\ \vec{\phi}^{(i)}(x_0, t) &= \vec{\phi}^{(i)}(X, t) = \vec{0}, \\ \vec{\phi}^{(i)}(x, t_c) &= \vec{\psi}^{(i)}(x), \end{aligned} \quad (44)$$

with initial conditions

$$\psi^{(1)}(x) = w(x), \quad \psi^{(2)}(x) = (A^\top(x)\vec{w}(x))_x. \quad (45)$$

5 Numerical Results

This section investigates the accuracy of the error estimates laid out in sections 4.1 and 4.2. One example of the heat equation is done in Section 5.1. We start off with results concerning the the heat equation in Section 5.1. The remainder of the examples deal with the linearized shallow water equations with different bathymetries and initial conditions. In all cases we consider one dimension in space; $\Omega = [x_0, X]$.

In the examples, the following notation is used. The sub-intervals in the spatial mesh have length $(X - x_0)/N_x$. The sub-intervals in the time mesh have length $(T - t_0)/N_t$. If a problem has $N_x = N_t$, we denote both as N . Forward problems are solved using a space-time Galerkin method, from Section 2.2. In most examples, the same degree for the space and time discretizations are used, with the exception of Section 5.4.1 Adjoint problems are solved on the same space-time mesh as the forward problem, using a Galerkin Finite Element Method of one degree higher, in both space and time, unless otherwise noted.

5.1 Heat Equation

Consider the one dimensional heat equation

$$\begin{aligned} u_t - u_{xx} &= \sin(\pi x)(\pi^2 \cos(t) - \sin(t)) & x \in [0, 1], t \in [0, 0.5], \\ u(0, t) &= u(1, t) = 0 & t \in [0, 0.5], \\ u(x, 0) &= \sin(\pi x) & x \in [0, 1]. \end{aligned} \quad (46)$$

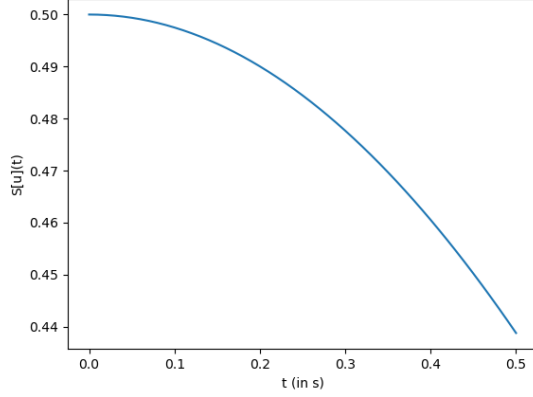
This problem has the analytic solution $u(x, t) = \cos(t) \sin(\pi x)$. Let the functional in (15) be

$$S[u](t) = (w(\cdot), u(\cdot, t)) = (\sin(\pi(\cdot)), u(\cdot, t)), \quad (47)$$

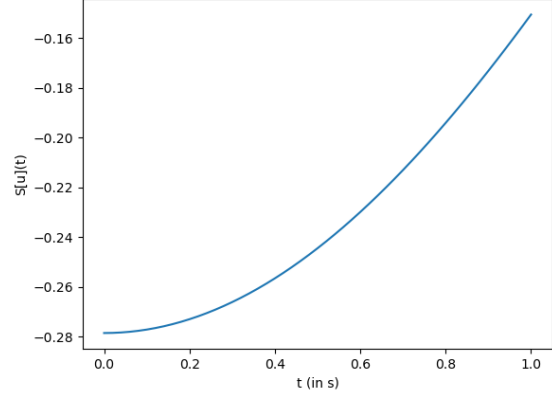
and let the threshold value be $R = 0.47$. The true values of the functional are graphed in Figure 2a.

The initial conditions (42) needed for the adjoint problems are

$$\psi^{(1)}(x) = w(x) = \sin(\pi x), \quad \psi^{(2)}(x) = w_{xx} = -\pi^2 \sin(\pi x) \quad (48)$$



(a) True values of functional S for example in Section 5.1.



(b) True values of functional S for example in Section 5.2.

Figure 2

The problem (46) is solved using the cG(1,1) and cG(2,2) methods with different uniform meshes. The results are given in Tables 1 and 2, respectively, which show that the error decreases as the mesh is refined. The effectivity ratios are close to 1 signifying accurate error estimates.

N	t_c	e_Q	ρ_{eff}
50	0.346346	1.808×10^{-3}	0.993
100	0.347711	4.546×10^{-4}	0.998
200	0.348053	1.129×10^{-4}	0.999
400	0.348137	2.844×10^{-5}	0.998

Table 1: Results for example in Section 5.1 using cG(1,1) with different mesh sizes. The true QoI is $t_t = 0.34816602$.

N	t_c	e_Q	ρ_{eff}
50	0.348166	9.6030×10^{-8}	1.000
100	0.348166	5.8411×10^{-9}	1.000
200	0.348166	5.0444×10^{-10}	1.000
400	0.348166	-6.0879×10^{-11}	0.992

Table 2: Results for example in Section 5.1 using cG(2,2) with different mesh sizes. The true QoI is $t_t = 0.34816602$.

5.2 Linearized SWE: Example 1

Consider the linearized SWEs (9) over the domain $(x, t) \in [0, 10] \times [0, 1]$ with right hand side

$$\vec{f} = \begin{pmatrix} f_1 \\ f_2 \end{pmatrix} = \begin{pmatrix} -\sin(t)\sin(\pi x) + \pi \cos(t)\cos(\pi x) \\ -\sin(t)\sin(\pi x) + \pi \cos(t)\cos(\pi x) \end{pmatrix}, \quad (49)$$

with a bathymetry of $B(x) = 0$ and a rest-state height of $\bar{\eta} = 2$. Set Dirichlet boundary conditions of $\vec{u}(x_0, t) = \vec{u}(X, t) = (2, 0)^\top$, and initial conditions $\vec{u}(x, t) = \vec{u}(X, t) = (2 + \sin(\pi x), \sin(\pi x))^\top$.

This problem has the analytic solution

$$\vec{u}(x, t) = \begin{pmatrix} \eta(x, t) \\ \mu(x, t) \end{pmatrix} = \begin{pmatrix} 2 + \cos(t)\sin(\pi x) \\ \cos(t)\sin(\pi x) \end{pmatrix}. \quad (50)$$

To define the QoI, let $R = -0.19$ and let weight function in (15) be $\vec{w}(x) = (0, w_2(x))$ where

$$w_2(x) = \begin{cases} 10(x-5)^2(x-6)^2 & 5 < x < 6, \\ 0 & x \leq 5, \\ 0 & x \geq 6. \end{cases} \quad (51)$$

The true values of the functional $S[u](t) = (w(\cdot), u(\cdot, t))$ are graphed in Figure 2b.

The initial conditions (45) for the adjoint problems are

$$\vec{\psi}^{(1)}(x, t_c) = (0, w_2(x))^\top, \quad \vec{\psi}^{(2)}(x, t_c) = (g\bar{h}(x)w_{2,x}(x), 0)^\top. \quad (52)$$

This problem is solved using the cG(2,2) method with several uniform meshes. Results are given in Table 3. Again the effectivity ratios ρ_{eff} are close to 1, meaning the error estimate is accurate.

N	t_c	e_Q	ρ_{eff}
50	0.819712	1.647×10^{-4}	1.001
100	0.819866	1.067×10^{-5}	1.000
200	0.819876	6.724×10^{-7}	1.000
400	0.819876	4.203×10^{-8}	1.000

Table 3: Results for example in Section 5.2. The true QoI is $t_t = 0.81987644$

5.3 Linearized SWE: Example 2

Now consider the equations (9) over the domain $[x_0, X] \times [t_0, T] = [0, 400] \times [0, 200]$, with right hand side $\vec{f} = (0, 0)^\top$. The bottom profile is flat with $B(x) = 0$. The rest-state height is $\bar{\eta} = 1$. Set Dirichlet boundary conditions only on the momentum, $\mu(x_0, t) = \mu(X, t) = 0$, and set an initial condition of $u(x, t_0) = (\eta_0(x), 0)^\top$, where

$$\eta_0(x) = \begin{cases} \frac{0.4}{390625}(x-100)^2(x-150)^2 & 100 < x < 150, \\ 0 & x \leq 100, \\ 0 & x \geq 150. \end{cases} \quad (53)$$

For the QoI (2), let $R = 2$ and the weight function in the functional (15) be $\vec{w} = (w_1(x), 0)^\top$ where

$$w_1(x) = \begin{cases} \frac{1}{200000}(x-160)^2(x-200)^2 & 160 < x < 200, \\ 0 & x \leq 160, \\ 0 & x \geq 200. \end{cases} \quad (54)$$

Since an analytic solution u is unavailable, a reference solution u is computed using a much smaller mesh-size than the forward solution. Here, the reference solution uses a mesh-size of $N_{ref} = 800$. Values of the functional $S[u](t)$ are graphed in Figure 3a.

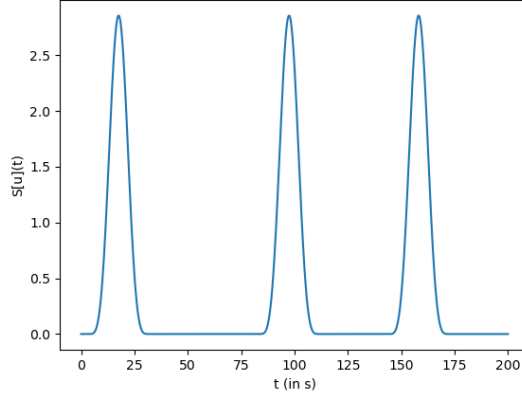
The initial conditions (45) for the adjoint problems are

$$\vec{\psi}^{(1)}(x, t_c) = (w_1(x), 0)^\top, \quad \vec{\psi}^{(2)}(x, t_c) = (0, w_{1,x}(x))^\top. \quad (55)$$

The forward problem is solved using the cG(2,2) method, with different uniform meshes. Results are given in Table 4 again showing that the effectivity ratios are close to 1.

N	t_c	e_Q	ρ_{eff}
50	14.0923	-9.095×10^{-2}	1.005
100	14.0073	-5.900×10^{-3}	1.000
200	14.0018	-3.964×10^{-4}	0.999
400	14.0014	-2.218×10^{-5}	0.999

Table 4: Results for example in Section 5.3. The reference QoI is $t_t = 14.001387$.



(a) Reference values of functional S for example in Section 5.3.

Figure 3

5.4 Linearized SWE: Example 3

This example introduces a non-flat sea floor. Consider the homogeneous, linearized SWEs (9) over domain $[x_0, X] \times [t_0, T] = [0, 400000] \times [0, 4200]$.

The bathymetry of the problem represents a continental shelf in the ocean that is continuous and linear:

$$B(x) = \begin{cases} -200 & x \leq 25000 \\ -0.152x + 3600 & 25000 < x < 50000 \\ -4000 & x \geq 50000. \end{cases} \quad (56)$$

The function $B(x)$ is shown in Figure 4a. Use a rest-state height of $\bar{\eta} = 1$. Set Dirichlet boundary conditions only on the momentum, $\mu(x_0, t) = \mu(X, t) = 0$, and set an initial condition of $u(x, t_0) = (\eta_0(x), 0)^\top$, where

$$\eta_0(x) = \begin{cases} \frac{0.4}{25000^4} (x - 100000)^2 (x - 150000)^2 & 100000 < x < 150000, \\ 0 & x \leq 100000, \\ 0 & x \geq 150000. \end{cases} \quad (57)$$

To define the QoI (2), let $R = 1000$, and let the weight function in (15) be $\vec{w}(x) = (w_1(x), 0)^\top$ where

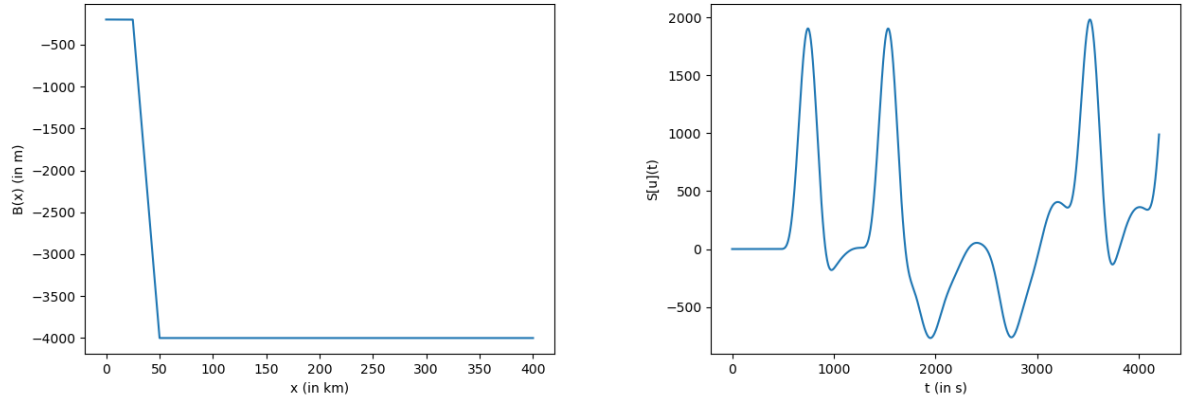
$$w_1(x) = \begin{cases} \frac{1}{7500^4} (x - 10000)^2 (x - 25000)^2 & 10000 < x < 25000, \\ 0 & x \leq 10000, \\ 0 & x \geq 25000. \end{cases} \quad (58)$$

A reference solution u is computed using a mesh with $N_{ref} = 1280$ sub-intervals. Values of the functional $S[u](t)$ are graphed in Figure 4b.

The initial conditions (45) for the adjoint problems are

$$\vec{\psi}^{(1)}(x, t_c) = (w_1(x), 0)^\top, \quad \vec{\psi}^{(2)}(x, t_c) = (0, w_{1,x}(x))^\top. \quad (59)$$

The forward problem is solved using the cG(2,2) method, with different uniform meshes. The results are in Table 5. In Table 5, the effectivity ratios are again close to 1 signifying accurate error estimates.



(a) Figure depicting bathymetry for example in Section 5.4 (b) Reference values of functional S for example in Section 5.4

Figure 4

N	t_c	e_Q	ρ_{eff}
80	651.267	-3.647×10^{-1}	1.002
160	650.975	-7.329×10^{-2}	1.000
320	650.907	-4.970×10^{-3}	1.000
640	650.902	3.672×10^{-4}	1.000

Table 5: Results for example in Section 5.4. Reference QoI is $t_t = 650.90208$.

5.4.1 Effects of accuracy of forward solution

This section investigates how the accuracy of the error estimate changes when the forward problem is solved using a lower degree Galerkin method. In Section 5.4, both spatial and temporal basis functions were degree 2. This example uses the same problem as Section 5.4, however when solving the forward problem the degree of the spatial basis functions is lowered to 1.

The results are presented in Table 6. Notice that the errors e_Q are much larger than in Section 5.4. Even so, effectivity ratios are close to 1 and the estimates are accurate.

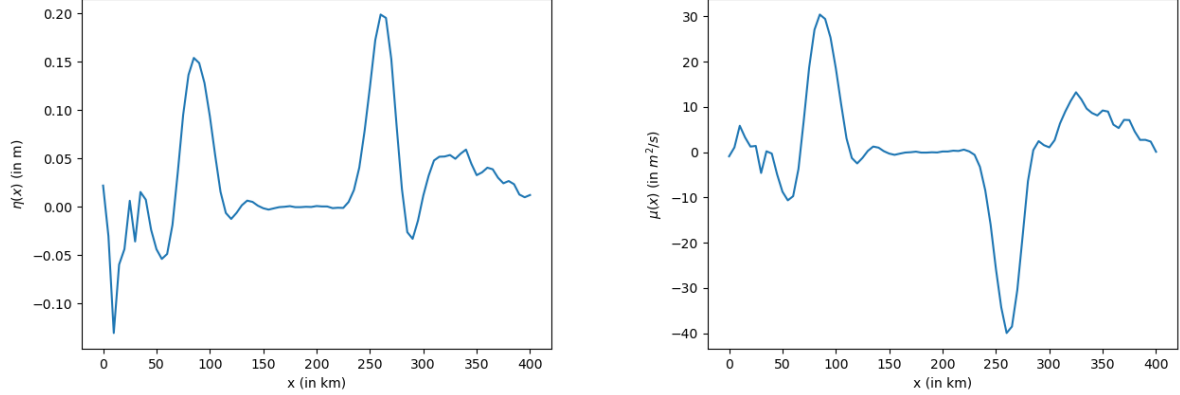
N	t_c	e_Q	ρ_{eff}
80	643.874	6.922×10^1	1.022
160	650.852	-5.536×10^{-2}	1.014
320	650.802	-5.360×10^{-3}	1.002
640	650.795	1.889×10^{-3}	0.997

Table 6: Results for example in Section 5.4.1. Reference QoI is $t_t = 650.79647$.

5.5 Linearized SWE: Example 4

This example allows a longer amount of time to pass before the threshold value is achieved. This is achieved by running the problem in Section 5.4 for $t = 2100$ seconds. The solution at $t = 2100$ is used as the initial conditions (η_0, μ_0) for the problem in this Section. The graphs of η_0 and μ_0 are shown in Figures 5a and 5b, respectively. All other aspects of the problem in Section 5.4 are retained. A graph of the functional $S[u](t)$ for this problem is found in Figure 1.

The reference solution is solved using a mesh with $N_{ref} = 1280$ sub-intervals in space and time. The results are in Table 7. The effectivity ratios are again close to 1 signifying accurate error estimates.



(a) Initial condition for fluid height for example in Section 5.5 (b) Initial condition for momentum for example in Section 5.5

Figure 5

N	t_c	e_Q	ρ_{eff}
80	1314.03	-9.870×10^{-1}	1.004
160	1313.22	-1.802×10^{-1}	1.000
320	1313.05	-1.287×10^{-2}	0.999
640	1313.04	-5.871×10^{-4}	1.000

Table 7: Results for example in Section 5.5. Reference QoI is $t_t = 1313.0382$.

5.6 Linearized SWE: Example 5

This Section investigates another non-flat bathymetry. Again consider the homogeneous, linearized SWEs (9) over the domain $[x_0, X] \times [t_0, T] = [0, 400000] \times [0, 4200]$. The bottom profile is a simplified representation of an obstruction on the sea floor, e.g. a reef, and is given as

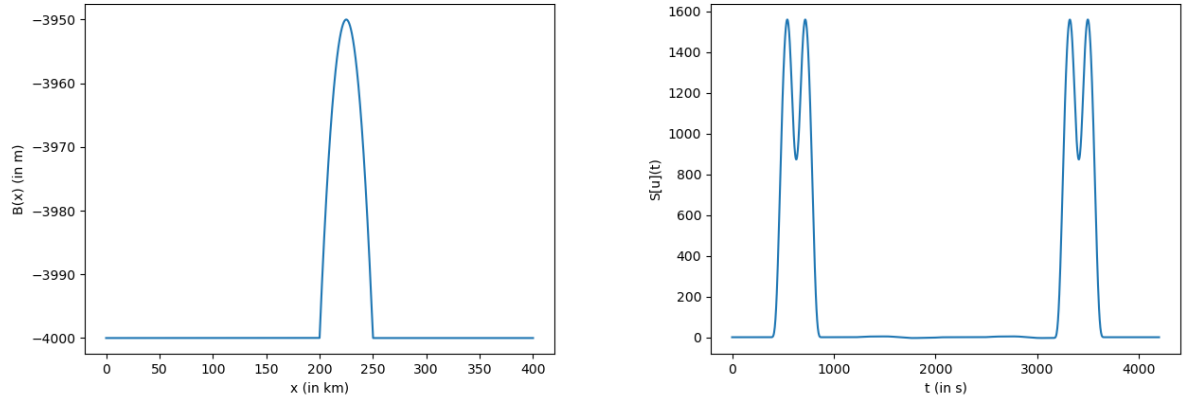
$$B(x) = \begin{cases} -4000 & x \leq 25000 \\ \frac{-50}{25000^2}(x - 200000)(x - 250000) & 200000 < x < 250000 \\ -4000 & x \geq 500000 \end{cases}. \quad (60)$$

The function $B(x)$ is depicted in Figure 6a. Use a rest-state height of $\bar{\eta} = 1$. Set Dirichlet boundary conditions on the momentum, $\mu(x_0, t) = \mu(X, t) = 0$, and set an initial condition of $u(x, t_0) = (\eta_0(x), 0)^\top$, where

$$\eta_0(x) = \begin{cases} \frac{0.4}{25000^4}(x - 100000)^2(x - 150000)^2 & 100000 < x < 150000 \\ 0 & x \leq 100000 \\ 0 & x \geq 150000 \end{cases}. \quad (61)$$

To set up the QoI (2), let $R = 1000$ and let the weight function in the functional (15) be $\vec{w}(x) = (w_1(x), 0)^\top$ with

$$w_1(x) = \begin{cases} \frac{1}{7500^4}(x - 10000)^2(x - 25000)^2 & 10000 < x < 25000 \\ 0 & x \leq 10000 \\ 0 & x \geq 25000 \end{cases}. \quad (62)$$



(a) Figure depicting bathymetry for example in Section 5.6 (b) Reference values of functional S for example in Section 5.6

Figure 6

The reference solution is computed on a mesh with $N_{ref} = 1280$ sub-intervals. The graph of the reference functional $S[u](t)$ is found in Figure 6b.

The initial conditions (45) for the adjoint problems are

$$\vec{\psi}^{(1)}(x, t_c) = (w_1(x), 0)^\top, \quad \vec{\psi}^{(2)}(x, t_c) = (0, w_{1,x}(x))^\top. \quad (63)$$

The forward problem is solved using the cG(2,2) method with several uniform meshes. Results are provided in Table 8 showing that the effectivity ratios, ρ_{eff} , are close to 1 which indicates that the error estimates are accurate.

N	t_c	e_Q	ρ_{eff}
80	489.353	-3.3980×10^0	1.016
160	485.870	8.4807×10^{-2}	0.999
320	485.951	4.4824×10^{-3}	1.000
640	485.954	7.1455×10^{-4}	1.000

Table 8: Results for example in Section 5.6. Reference QoI is $t_t = 485.95515$.

6 Conclusions

Accurate *a posteriori* error estimates using Taylor's Theorem and adjoint based error analysis are devised in the context of PDEs for the non-standard QoI; the first time a given functional reaches a threshold value. Recall that a non-standard QoI is a QoI that cannot be represented as a bounded functional of the solution of the forward problem. These error estimates are shown for both the heat equation (hyperbolic) and SWE (parabolic) time evolution PDEs. The SWEs were investigated with different mesh sizes, initial conditions, and bathymetries. In all cases, the error estimates of the non-standard QoI were accurate.

Acknowledgments

J. Chaudhry's work is supported by the NSF-DMS 1720402. S. Tavener's work is supported by NSF-DMS 1720473.

References

- [1] M. Ainsworth and T. Oden. *A posteriori error estimation in finite element analysis*. John Wiley-Teubner, 2000.
- [2] W. Bangerth and R. Rannacher. *Adaptive Finite Element Methods for Differential Equations*. Birkhauser Verlag, 2003.
- [3] T. J. Barth. *A posteriori Error Estimation and Mesh Adaptivity for Finite Volume and Finite Element Methods*, volume 41 of *Lecture Notes in Computational Science and Engineering*. Springer, New York, 2004.
- [4] R. Becker and R. Rannacher. An optimal control approach to *a posteriori* error estimation in finite element methods. *Acta Numerica*, pages 1–102, 2001.
- [5] Oliver Bühler. A shallow-water model that prevents nonlinear steepening of gravity waves. *Journal of the Atmospheric Sciences*, 1998.
- [6] Yang Cao and Linda Petzold. *A posteriori* error estimation and global error control for ordinary differential equations by the adjoint method. *SIAM Journal on Scientific Computing*, 26(2):359–374, 2004.
- [7] V. Carey, D. Estep, and S. Tavener. *A posteriori* analysis and adaptive error control for multiscale operator decomposition solution of elliptic systems I: Triangular systems. *SIAM Journal on Numerical Analysis*, 47(1):740–761, 2008.
- [8] J. H. Chaudhry, D. Estep, V. Ginting, and S. Tavener. *A posteriori* analysis for iterative solvers for non-autonomous evolution problems. *SIAM Journal on Uncertainty Quantification*, 3, 2015.
- [9] J. H. Chaudhry, J.N. Shadid, and T. Wildey. *A posteriori* analysis of an IMEX entropy-viscosity formulation for hyperbolic conservation laws with dissipation. *Applied Numerical Mathematics*, 135, 2019.
- [10] J.H. Chaudhry. *A posteriori* analysis and efficient refinement strategies for the Poisson–Boltzmann equation. *SIAM Journal on Scientific Computing*, 40(4):A2519–A2542, 2018.
- [11] J.H. Chaudhry, J.B. Collins, and J.N. Shadid. *A posteriori* error estimation for multi-stage Runge-Kutta IMEX schemes. *Applied Numerical Mathematics*, 117:36–49, Jul 2017.
- [12] J.H. Chaudhry, D. Estep, V. Ginting, J.N. Shadid, and S. Tavener. *A posteriori* error analysis of IMEX multi-step time integration methods for advection–diffusion–reaction equations. *Computer Methods in Applied Mechanics and Engineering*, 285:730–751, 2015.
- [13] J.H. Chaudhry, D. Estep, V. Ginting, and S.J. Tavener. *A posteriori* analysis of an iterative multi-discretization method for reaction-diffusion systems. *Computer Methods in Applied Mechanics and Engineering*, 267:1–22, 2013.
- [14] J.H. Chaudhry, D. Estep, and M. Gunzburger. Exploration of efficient reduced-order modeling and a posteriori error estimation. *International Journal for Numerical Methods in Engineering*, 111(2):103–122, 2017.
- [15] J.H. Chaudhry, D. Estep, and S. Tavener. *A posteriori* error analysis for Schwarz overlapping domain decomposition methods. *arXiv e-prints*, page arXiv:1907.01139, Jul 2019.
- [16] J.H. Chaudhry, D. Estep, S. Tavener, V. Carey, and J. Sandelin. *A posteriori* error analysis of two-stage computation methods with application to efficient discretization and the Parareal algorithm. *SIAM Journal on Numerical Analysis*, 54(5):2974–3002, 2016.
- [17] J.H. Chaudry, D. Estep, Z. Stevens, and S. Tavener. Error estimation and uncertainty quantification for first time to a threshold value. *BIT Numerical Mathematics*, 61:275–307, 2021.

- [18] K.A. Cliffe, J. Collis, and P. Houston. Goal-oriented *a posteriori* error estimation for the travel time functional in porous media flows. *SIAM Journal of Scientific Computing*, 37(2):B127–B152, 2015.
- [19] J. B. Collins, D. Estep, and S. Tavener. *A posteriori* error analysis for finite element methods with projection operators as applied to explicit time integration techniques. *BIT Numerical Mathematics*, 55(4):1017–1042, 2015.
- [20] James B. Collins, Don Estep, and Simon Tavener. *A posteriori* error estimation for the Lax–Wendroff finite difference scheme. *Journal of Computational and Applied Mathematics*, 263:299–311, 2014.
- [21] B.N. Davis and R.J. LeVeque. Adjoint methods for guiding adaptive mesh refinement in tsunami modeling. *Pure and Applied Geophysics*, 173:4055–4074, 2016.
- [22] M. Delfour, W. Hager, and F. Trochu. Discontinuous Galerkin methods for ordinary differential equations. *Math. Comp.*, 36(154):455–473, 1981.
- [23] M. C. Delfour and F. Dubeau. Discontinuous polynomial approximations in the theory of one-step, hybrid and multistep methods for nonlinear ordinary differential equations. *Math. Comp.*, 47(175):169–189, S1–S8, 1986.
- [24] K. Eriksson, D. Estep, P. Hansbo, and C. Johnson. Introduction to adaptive methods for differential equations. In *Acta Numerica, 1995*, Acta Numerica, pages 105–158. Cambridge Univ. Press, Cambridge, 1995.
- [25] K. Eriksson, C. Johnson, and A. Logg. Explicit time-stepping for stiff ODEs. *SIAM Journal on Scientific Computing*, 25(4):1142–1157, 2004.
- [26] D. Estep. *A posteriori* error bounds and global error control for approximation of ordinary differential equations. *SIAM J. Numer. Anal.*, 32(1):1–48, 1995.
- [27] D. Estep. A short course on duality, adjoint operators, Green’s functions, and *A Posteriori* error analysis. Unpublished, 2004.
- [28] D. Estep. Error estimates for multiscale operator decomposition for multiphysics models. In J. Fish, editor, *Multiscale methods: bridging the scales in science and engineering*. Oxford University Press, USA, 2009.
- [29] D. Estep, V. Ginting, and S. Tavener. *A posteriori* analysis of a multirate numerical method for ordinary differential equations. *Computer Methods in Applied Mechanics and Engineering*, 223:10–27, 2012.
- [30] D. Estep, M. Holst, and D. Mikulencak. Accounting for stability: *a posteriori* error estimates based on residuals and variational analysis. *Comm. Numer. Methods Engrg.*, 18:15–30, 2002.
- [31] D. Estep, M. Larson, and R. Williams. Estimating the error of numerical solutions of systems of reaction-diffusion equations. *Memoirs of the American Mathematical Society*, 696, 07 2000.
- [32] Lawrence C. Evans. *Partial differential equations*. American Mathematical Society, 2010.
- [33] Harry Yeh George F. Carrier. Tsunami propagation from a finite source. *Computer Modeling in Engineering & Sciences*, 2005.
- [34] M. B. Giles and E. Süli. Adjoint methods for pdes: *a posteriori* error analysis and postprocessing by duality. *Acta Numerica*, 11(1):145–236, 2002.
- [35] A. Johansson, J. H. Chaudhry, V. Carey, D. Estep, V. Ginting, M. Larson, and S.J. Tavener. Adaptive finite element solution of multiscale PDE–ODE systems. *Computer Methods in Applied Mechanics and Engineering*, 287:150–171, 2015.
- [36] Anders Logg. Multi-adaptive time integration. *Appl. Numer. Math.*, 48(3-4):339–354, mar 2004.

A Theorem 3

Theorem 3. For semi-linear time evolution PDEs

$$u_t(x, t) + Lu(x, t) = f(u, x, t) \quad x \in \Omega, \quad t \in (t_0, T], \quad (64)$$

the error in the QoI (2) is given as

$$e_Q = t_t - t_c = \frac{(w(\cdot), e(\cdot, t_c)) + (w(\cdot), \mathcal{R}_1(\cdot, t_c, t_t))}{(L_2 w(\cdot), L_1 U(\cdot, t_c)) - (w(\cdot), f(U, \cdot, t_c)) - (w(\cdot) \nabla_u f(U, \cdot, t_c), e(\cdot, t_c)) + (L_2 w(\cdot), L_1 e(\cdot, t_c)) - (w(\cdot), \mathcal{R}_2(u, U, \cdot, t_c))}. \quad (65)$$

Where $e(x, t) = u(x, t) - U(x, t)$, and the two remainders are $\mathcal{R}_1(x, t_c, t_t) = \mathcal{O}((t_t - t_c)^2)$ and $\mathcal{R}_2(u, U, x, t_c) = \mathcal{O}((u - U)^2)$.

Proof. Follow the proof of Theorem 1 up until (25), replacing $f(x, t)$ with $f(u, x, t)$. From there, use Taylor's Theorem once more to expand $f(u, x, t_c)$ around U :

$$(w(\cdot), f(u, \cdot, t_c)) = (w(\cdot), f(U, \cdot, t_c)) + (w(\cdot), \nabla_u f(U, \cdot, t_c) e(\cdot, t_c)) + (w(\cdot), \mathcal{R}_2(u, U, \cdot, t_c)), \quad (66)$$

$$= (w(\cdot), f(U, \cdot, t_c)) + (w(\cdot) \nabla_u f(U, \cdot, t_c), e(\cdot, t_c)) + (w(\cdot), \mathcal{R}_2(u, U, \cdot, t_c)), \quad (67)$$

where the remainder $\mathcal{R}_2(u, U, x, t_c)$ is of order $\mathcal{O}((u - U)^2)$. Plugging (67) into (25) and putting that back into (23) yields the final result. \square

As before, obtain an approximation of e_Q by setting \mathcal{R}_1 and \mathcal{R}_2 to zero. This approximation requires an additional adjoint problem to be solved:

Third adjoint problem To estimate $(w(\cdot) \nabla_u f(U, \cdot, t_c), e(\cdot, t_c))$ solve (70) with initial condition $\psi(x) = \psi^{(3)}(x) = w(x) \nabla_u f(U, x, t_c)$. Using the solution $\phi^{(3)}$ in (69) yields

$$\mathcal{E}_3 \approx (\psi^{(3)}(\cdot), e(\cdot, t_c)) = (w(\cdot) \nabla_u f(U, \cdot, t_c), e(\cdot, t_c)). \quad (68)$$

A Theorem 4

The adjoint problems are adjusted to deal with the possible non-linearity of the function f . In particular, the right-hand side of the adjoint equation is obtained by linearizing f .

Theorem 4. Given a numerical solution $U(x, t)$ to (64) and data $\psi(x)$, the error $(\psi(\cdot), e(\cdot, \hat{t}))$ for $\hat{t} \in (t_0, T]$ is given by

$$(\psi(\cdot), e(\cdot, \hat{t})) = (\phi(\cdot, t_0), e(\cdot, t_0)) + \int_{t_0}^{\hat{t}} (\phi(\cdot, \hat{t}), f(U, \cdot, \hat{t}) - U_t(\cdot, \hat{t})) dt - \int_{t_0}^{\hat{t}} (L_2 \phi(\cdot, \hat{t}), L_1 U(\cdot, \hat{t})) dt \quad (69)$$

where $\phi(x, t)$ is the solution of the adjoint problem

$$\begin{aligned} -\phi_t(x, t) - L^* \phi(x, t) &= A_{u, U}^* \phi(x, t), \quad x \in \Omega, \quad t \in [t_0, \hat{t}) \\ \phi(x, t)|_{\partial\Omega} &= 0, \quad t \in [t_0, \hat{t}), \\ \phi(x, \hat{t}) &= \psi(x), \quad x \in \Omega. \end{aligned} \quad (70)$$

The operator $A_{u, U}^*$ is the adjoint of the linear operator

$$A_{u, U} = \int_0^1 \frac{df}{dz}(z, x, t) ds, \quad (71)$$

and $z = su + (1 - s)U$.

The operator $A_{u,U}$ has the property that

$$A_{u,U}e(x,t) = f(u,x,t) - f(U,x,t). \quad (72)$$

Proof. This proof mimics the proof of Theorem 2. Start with the adjoint problem (70), and use the property (72) to cancel terms. □

In practice, since operator $A_{u,U}$ requires the true solution to (64), it is approximated by

$$A_{u,U} \approx \nabla_u f(U,x,t). \quad (73)$$

With this, the right side of the adjoint equation (70) is approximated by

$$A_{u,U}^* \phi(x,t) \approx (\nabla_u f(U,x,t))^\top \phi(x,t). \quad (74)$$